BA-92-71
UPR-0218E

Atmospheric Neutrino Data and Neutrino Oscillations

W. Frati, [2*] T.K. Gaisser, [1*] A.K. Mann, [2*] Todor Stanev [1**]

[1]Bartol Research Institute
University of Delaware
Newark, DE 19716

[2]Department of Physics
University of Pennsylvania
Philadelphia, PA 19104

Abstract

Several calculations of the upward through-going and stopping muon fluxes produced by atmospheric, or cosmic ray, neutrinos interacting in the material surrounding underground detectors are compared and the uncertainties in the calculations estimated. We evaluate the implications for neutrino oscillations of the measured and calculated upward muon fluxes in relation to the neutrino oscillation interpretation of the atmospheric neutrino–induced interactions totally contained within the underground detectors. It appears that the region of the $\Delta m^2, \sin^2 2\theta$ parameter space excluded by previous analyses of the upward through-going muons has been overestimated, and that a more likely representation is consistent with the contained event result. In contrast, the region delineated by comparison of the observed and calculated stopping fractions is less ambiguous and comparable in quality with that obtained from the totally contained event samples.

December 8, 1992

*Supported in part by the U.S. Department of Energy

**Supported in part by the U.S. National Science Foundation

Introduction

At hand now are neutrino data induced by extra-terrestrial neutrino sources that are improved in quantity and quality over the data available a few years ago. In addition to important solar neutrino results, there are relatively large atmospheric neutrino data samples from which significant conclusions regarding neutrino mass and mixing may tentatively be extracted. Atmospheric, or cosmic ray, muons and neutrinos are produced by the interactions of the primary components of the cosmic ray flux with the earth's atmosphere, giving rise to pions and kaons which decay to give the muons and neutrinos observed on earth. The muon flux has been studied for more than a half century; the neutrino flux for less than twenty years and with large event samples only in the last decade.

The atmospheric neutrino data of most statistical significance have so far been acquired in large imaging water Cherenkov counters [1,2,3] located relatively deep underground; informative data samples have also been obtained with smaller, differently constituted detectors[4,5]. There are two distinct experimental methods of studying atmospheric neutrinos. They may be detected (i) by means of their interactions within a massive target-detector which contains the neutrino-nucleus interaction vertex and all the interaction products (known as contained events); and (ii) by means of the muons produced in neutrino interactions with the matter surrounding the detector from as far away as several kilometers, with the product muons either completely traversing or stopping in the detector (so-called upward-going muon events). It is the purpose of this paper to compare the data from the two experimental methods and thereby to investigate the internal consistency of conclusions relating to neutrino oscillations drawn from the totality of the data.

Contained Event and Upward-Going Event Data

The contained events are largely due to neutrinos in the energy interval $0.3 \lesssim E_\nu \lesssim 1.5$ GeV, and they exhibit single or multiple Cherenkov rings. Approximately 75% of the single ring events in the detector are the result of quasielastic neutrino reactions, $\nu_\mu n \rightarrow \mu^- p$ ($\bar{\nu}_\mu p \rightarrow$

$\mu^+ n$) and $\nu_e n \rightarrow e^- p$ ($\bar{\nu}_e p \rightarrow e^+ n$) in which the recoil proton is below Cherenkov threshold, and 14% result from single pion production in which either the pion or lepton is below the threshold for Cherenkov radiation.The remainder is attributed to weak neutral current reactions in which one hadron is above Cherenkov threshold. It is possible to determine their particle type (e or μ/π), and respective momentum and zenith angle distributions, as well as the number of μ-decays in the total event sample. Roughly, one-half of the observed contained event sample is produced by neutrinos with zenith angles less than 90° ("downward"), and one-half by neutrinos with larger zenith angles ("upward"); the former having traveled a distance of $\sim$ 10–100 km from their origin in the atmosphere to the detector, and the latter a distance of $\sim (1\text{–}13) \times 10^3$ km to reach the detector. The results from the contained single-ring event data have recently been summarized [6]. Briefly, the data from the two multikiloton imaging water Cherenkov detectors, Kamiokande and IMB, are in excellent agreement with each other. Momentum distributions of electron and muon single ring events, the absolute electron and muon event rates, the zenith angle distributions, and the fraction of muon decays in the total sample have all been measured.

The most striking feature of the contained event sample reported both by IMB and Kamiokande is that the observed ratio of muon-like to electron-like events is significantly less than expected, as summarized here in Table I [6]. The calculations on which this conclusion is based involve three factors: (1) the spectra of atmospheric $\nu_\mu(\bar{\nu}_\mu)$ and $\nu_e(\bar{\nu}_e)$, (2) properties of neutrino interactions in water and (3) simulation of the detector response. One possible interpretation of the anomaly is that the neutrino flux differs from expectation because of the presence of neutrino oscillations. Fig. 1 [2,6] shows the region in the $\Delta m^2 - \sin^2 2\theta$ parameter space that would explain the observation as ν_μ disappearance to a ν_τ or a sterile neutrino. An explanation in terms of $\nu_\mu - \nu_e$ oscillations is also possible, but for this channel most of the "allowed" region is excluded by other experiments [2]. It has been pointed out [7,8,9] that under some circumstances neutrino oscillations as the explanation of the contained event data would imply also an anomaly in the neutrino-induced upward muons. Our goal here is

to explore this possibility in detail.

The muons studied in method (ii) are necessarily upward-going ($\theta_Z > 90°$) since the downward muon flux coming directly from the meson decays in the atmosphere is orders of magnitude larger than the downward muon signal from neutrino interactions in the surrounding matter. The calculated energies of atmospheric neutrinos giving rise to the contained events and to the observed upward stopping and through-going muons are shown in Fig.2, where it is seen that the mean energies of the neutrinos involved are approximately 0.8, 10 and 100 GeV, respectively. The information carried by the upward-going muons is their zenith angle distribution and total numbers stopping within the detector and traversing it. The results from the upward-going muon event data have also been published [7,8,9,10], and the measured absolute values of the through-going muon fluxes are in good agreement. This will be discussed below when the basis for comparing measurements made under differing experimental conditions is clarified.

There are several important differences between contained events and upward-going muons as probes of neutrino oscillations. First, the relative values of $< E_\nu/L >$ are $\gtrsim 10^{-4}$ GeV/km for the contained events, $\approx 10^{-3}$ for the stopping events, and $\approx 10^{-2}$ for the upward through-going events. This ratio sets the scale for the region in Δm^2 accessible to each of the samples through the factor $\sin^2 (1.27\Delta m^2 L/E)$ in the expression for the oscillation probability (see Eq. (2) below).

Second, in the contained event data, the ratio of the observed number of muons to the observed number of electrons is compared with the corresponding calculated ratio. In the observed ratio certain properties of the detector effectively cancel. Most importantly, in the calculated ratio the absolute values of the atmospheric ν_e and ν_μ fluxes are not required. There are several independent calculations of the atmospheric neutrino fluxes in the GeV range needed for the contained events [11,12,13,14,15]. The calculations that include the effect of muon polarization [16] all give values for the flux ratio $\phi(\nu_\mu + \bar{\nu}_\mu)/\phi(\nu_e + \bar{\nu}_e)$ within a range of 5%, as shown in Table II [17], despite differences among the absolute flux values

of as much as 30%. In the case of through-going upward muons the measured absolute muon flux is compared with the calculated absolute muon flux. To obtain the neutrino flux over the energy region indicated in Fig. 2, requires knowledge of the composition and absolute intensity of the primary components of cosmic rays, and of the details of the interactions of those components with the nuclei of the atmosphere, including the relative abundances of produced non-strange and strange mesons. To calculate the subsequent through-going muon flux requires the absolute cross sections for neutrino-nucleus reactions over the energy interval in Fig. 2 and detailed knowledge of energetic muon propagation in matter.

Uncertainties in the absolute values of the various quantities which enter the calculation of the upward through-going muon flux limit the conclusions about neutrino oscillations that can be otained by comparison of the observed and expected rates, even when experimental uncertainties are small. This point was recognized explicitly by Oyama et al.[10] who showed limits obtained under different assumptions concerning neutrino fluxes, neutrino cross sections and muon propagation. In this paper we explore the problem in detail using nucleon structure functions based on more recent measurements of neutrino cross sections and, more importantly, using a wider variety of neutrino flux calculations.

The calculation of the fraction of upward-going muons that stop in the detector is less demanding [8]. For example, because the stopping and through-going muons come from different ranges of neutrino energy, the calculation depends on the shape of the primary spectrum, but not its normalization. Similarly, the relative neutrino intensities and interaction cross sections in the two energy ranges of Fig. 2 are needed, but uncertainties in absolute scales largely cancel. One source of uncertainty that does not cancel in calculating the ratio of stopping to through-going muons is the relative production of kaons. As a consequence of kinematics, kaons are the dominant source of muon neutrinos in the 100 GeV range and above. Thus kaons contribute more to throughgoing muons ($\sim$ 50%) than to stopping muons ($\sim$ 25%).

Uncertainties in the Calculation of $\phi(\nu_\mu + \bar{\nu}_\mu)$

There have been several recent calculations of the neutrino fluxes, $\phi(\nu_\mu+\bar{\nu}_\mu)$ and $\phi(\nu_e+\bar{\nu}_e)$, in the higher energy regions of Fig. 2 [18,19,20,21]. The results for $\phi(\nu_\mu + \bar{\nu}_\mu)$ are shown in Fig. 3, which is compiled from tables in the cited references. Considering the absolute nature of the calculated fluxes in Fig. 3, there is satisfactory overall agreement among them. Some of the differences may arise from numerical approximations made in the calculational methods employed, and some from uncertainties in measurements of the underlying physical processes, e.g., the primary cosmic ray spectrum, inclusive cross sections, etc. Accordingly, the possible errors associated with the neutrino fluxes in Fig. 3 arise principally from uncertainties in and treatment of the input data common to all the calculations and hardly at all from lack of knowledge of the physical processes involved.

The question of the uncertainty in the calculated neutrino flux will be treated at length in reference [21] in which estimates of the uncertainties in the input data have been made and propagated through the calculation. Briefly, the 1σ error in the absolute intensity of the primary components is 15%, and the 1σ error in the uncorrelated absolute meson yields is also 15%. These contribute uncertainties of the same magnitudes to the absolute neutrino fluxes and, added in quadrature, give an expected 1σ uncertainty of 21% in the neutrino flux, i.e., about 2 times the range of values of the four calculations compared in Fig. 3. This is about what one would expect, in view of the fact that each of the calculations attempts to find the best value of each component of the input data. In addition, each calculation is required to be consistent with measurements [22] of the high energy muon flux.

Upward Through-Going Muon Fluxes

Given the calculated neutrino fluxes as functions of E_ν in Fig. 3, the upward through-going muon fluxes corresponding to each neutrino flux can in turn be calculated for a specific detector. The flux of muons with zenith angle θ and energy greater than E_μ at the detector

is given by

$$N_\mu(> E_\mu) = \sum_{\nu,\bar{\nu}} \int dE'_\mu \int dE_\nu \, R(E_\mu, E'_\mu) \frac{d\sigma_{\nu,\bar{\nu}}(E_\nu)}{dE'_\mu} \phi(E_\nu, \theta). \quad (1)$$

Here $d\sigma_{\nu,\bar{\nu}}(E_\nu)/dE'_\mu$ is the charged current cross section for a neutrino (antineutrino) of energy E_ν to produce a muon of energy E'_μ, and $R(E_\mu, E'_\mu)$ is the effective range in rock for the muon to survive with energy $> E_\mu$ [23]. The flux at the detector must be folded with the energy dependent threshold characteristic of each detector.

We show in Fig. 4 the four calculated muon zenith angular distributions compared with the distribution measured in the Kamiokande detector [9]. Note that both axes in Fig. 4 are labeled in absolute quantities and no renormalization of the calculated distributions has been applied. The shape of the muon angular distributions in Fig. 4 reflects primarily the angular dependence of the path lengths for decay of the parent mesons. The detailed response of the Kamiokande detector to upward muons has been included in our calculations [24]. For muon propagation we have used the recent work of Lipari & Stanev [23], which is valid for muon energies up to > 1000 TeV. In the present application, which involves muon energies $\lesssim$ 1 TeV, it gives results which are essentially identical to those of Lohmann *et al.* [25].

The choice of structure functions to be used in the calculation of the differential cross sections $d\sigma(E_\nu)/dE'_\mu$ for the charged current interactions of ν_μ and $\bar{\nu}_\mu$ requires more extensive discussion. The E_ν range of 10 to 1000 GeV corresponds to a modest range in $Q^2(\lesssim 1000\ GeV^2)$ for which propagator effects are relatively unimportant and small values of the proton momentum fraction x are not emphasized. We have compared four sets of structure functions [26,27,28,29]. All sets give similar results for the shape of the cross sections as a function of $y = 1 - E_\mu/E_\nu$. For comparison with measurements of upward muons we have used two sets of structure functions, EHLQ [26] and Owens [27]. We show results for the EHLQ structure functions – even though the data on which they are based have been superseded – because we are interested in comparing with previous analyses, all of which base their conclusions on this set of structure functions [7,8,9]. We use the Owens

set, which are appropriate for our leading order calculation and which give a somewhat closer representation of the measured total cross sections. We compare the cross sections derived from these structure functions with the neutrino scattering data summary in Fig. 5. The cross sections obtained from EHLQ set 2 are shown because both Kamiokande and IMB used those structure functions. (The EHLQ set 1 cross sections are about 3% lower than those from set 2.) Note that we evaluate the structure functions at $Q_0^2 = 5GeV^2$ when $Q^2 < Q_0^2$.

Quantitative results calculated for the Kamiokande detector are shown in Table III. The absolute muon fluxes in columns 2 (Owens structure functions) and 3 (EHLQ2 structure functions) of the table are calculated using the through-going muon event selection criteria appropriate to the Kamiokande detector. The muon fluxes vary over a range of 11% for a given set of structure functions. Use of the Owens [27] structure functions increases the predicted muon flux by approximately 12% as compared to EHLQ set 2. Values of the ratio $R = (meas/calc)$ are given in columns 4 and 5, with the measured Kamiokande result $(2.04 \pm 0.13) \times 10^{-13} cm^{-2} s^{-1} sr^{-1}$ [9] in the numerator. Observe that the entries in column 4 are consistent with an observed through-going muon rate that is less than the calculated rate.

The combinations of neutrino flux and structure functions marked with an asterisk in Table III were considered by Oyama[24], together with muon propagation from Lohmann[25], to compute rates of upward muons in Kamiokande. We also repeated our calculation with the other combinations of neutrino fluxes, structure functions and muon propagation used by Oyama; i.e., using the parton distributions due to Field and Feynman, [31] and the simple muon energy loss formula, $dE_\mu/dx = -\alpha - \beta E_\mu$. Within the Monte Carlo sampling statistics ($\sim 1\%$), all eight numbers agree with those of Oyama.

There are two other statistically significant sets of data on upward going muons. The Baksan detector [7] has measured the flux of upward going muons of energy > 1 GeV to be $(2.77 \pm 0.17) \times 10^{-13}$ $cm^{-2} sr^{-1} s^{-1}$. The IMB collaboration [32] has published the flux of upward going muons of energy > 2 GeV as $(2.26 \pm 0.11) \times 10^{-13} cm^{-2} sr^{-1} s^{-1}$. The data

of Kamiokande have an average muon pathlength in the detector, averaged over $\cos\theta_z$, of 12.2 m, corresponding to an effective muon energy threshold of 3 GeV.[9]

Although the three effective muon thresholds do not coincide we can compare them using the information summarized in Fig. 6. This figure shows the fluxes of upward going neutrino induced muons as a function of the muon threshold energy produced by the four neutrino fluxes [18,19,20,21] with the Owens [27] structure functions. While Fig. 6 shows the scaling factors for the angle averaged muon flux, the actual comparison was done by rescaling the data points with factors applicable to each angular bin for which the data were taken. The resulting angular distributions for muons of energy above 3 GeV from the three experiments are in good agreement. The rescaled angle averaged flux for $E_\mu > 3$ GeV for Baksan and IMB are respectively (2.08 ± 0.14) and $(1.92 \pm 0.11) \times 10^{-13}\text{cm}^{-2}\text{sr}^{-1}\text{s}^{-1}$, in good agreement with the Kamiokande value of (2.04 ± 0.13). Although scaling the data in this fashion is not exact, it is reliable since different neutrino fluxes produce a similar energy dependence of the muon fluxes, as can be verified by an inspection of Fig. 6. The shape of the curves in Fig. 6 is also independent of the choice of structure functions.

Upward Through-Going Muons and Neutrino Oscillations

We first analyze the implications of the results for $R(meas/calc)$ in Table III for neutrino oscillations in the ν_μ-disappearance channel. The ν_μ survival probability is given by

$$P(\nu_\mu \to \nu_\mu) = 1 - \sin^2 2\theta \sin^2 \left[1.27 \Delta m^2(\text{eV}^2) \frac{L(\text{km})}{E_\nu(\text{GeV})}\right] \qquad (2)$$

where θ is the vacuum mixing angle and L is the neutrino path length from production point to the detector. The denominator in the ratio $R(meas/calc)$ is obtained by accepting each Monte Carlo event that has previously passed the detector cuts with a probability given by Eq. 2. This procedure produces a sample of neutrinos properly weighted in energy and zenith angle. (The effective altitude for neutrino production in the atmosphere is taken to be 15 km.) To find the 90% c.l. of R (R_{90}) we use the error in the Kamiokande measurement (taken to be normally distributed) and attribute a normally distributed uncertainty of 21% (discussed

above) to the calculated muon flux to find the non-gaussian probability distribution of the values of R. For these error assignments the value of R_{90} (below which 90% of the area under the distribution is enclosed) is 0.775 times the central value of R in Table III.

We show in Fig. 7 the 90% c.l. contour obtained using the last entry on the fourth line of Table III, i.e., Kamioka data, Volkova neutrino flux and EHLQ2 structure functions. That contour, marked KVE, excludes a region similar to the 90% c.l. contour marked IMB [8] which is (curve A) in Fig. 2 of the IMB paper [8], and which was calculated under the same assumptions of neutrino flux and structure functions. The KVE contour is obtained by comparison to through-going data only and consequently does not extend to as small Δm^2 as the IMB contour, which includes lower energy, stopping muon data. If, however, the Bartol neutrino flux and Owens structure functions are used with the Kamioka data, the third entry on the first line of Table III, we obtain the 90% c.l. contour marked KBO in Fig. 7. A similar shift of the IMB contour would result from use of the larger neutrino flux and Owens structure functions. Finally, note that the contour KVE is different from the contour shown in the Kamiokande paper [9], marked KAM [9] in Fig. 7. Our analysis is based on R (meas/calc) while the Kamioka analysis primarily emphasizes comparison of the measured and calculated zenith angle distributions (see below).

The results in Fig. 7 indicate the wide range of $\Delta m^2, \sin^2 2\theta$ over which the contours derived from the IMB and Kamioka data may be located, depending on the assumed neutrino flux and nucleon structure functions from which the calculated through-going muon flux is determined. For reasons given above, it appears (i) that the region of the neutrino oscillation parameter space for ν_μ-disappearance previously excluded by analyses of upward through-going muons has been overestimated [7,8,9]; and (ii) that contours in the vicinity of KBO in Fig. 7 are more likely to represent the exclusion limits from a correctly calculated through-going muon flux.

Next, we consider an analysis which is sensitive to the measured angular distribution as well as $R(meas/calc)$. Fig. 8 shows the zenith angle distributions calculated for three values

of the parameter pairs $(\Delta m^2, \sin^2 2\theta)$ representative of values allowed by the contained event data in Fig. 2. These are compared with the no-oscillation distribution and the Kamiokande data [9]. Figs. 8a and 8b, respectively, are obtained with the same high and low combinations of neutrino flux and cross section used for Fig. 7. One sees that an analysis of Fig. 8a, based in part on the shape of the distribution as well as its integrated value, would be consistent with the three calculated distributions which include oscillations, although it would be unable to distinguish definitively among them. The situation is reversed in Fig. 8b where the data somewhat prefer the no-oscillation distribution over those that include oscillations. The χ^2 values for both figures are given in Table IV.

It is instructive also to consider fits based on angular distribution alone. This can be done by renormalizing each curve in Fig. 8 so that it gives the same total signal of upward muons as the data. The χ^2 values obtained in this way are also shown in Table IV. One sees that the discriminating power is now significantly less than when rate information is also used. The reason for this is suggested by considering how the angular distribution is affected by a presumed oscillation effect. Consider, for example, the distributions with $\Delta m^2 \leq 0.01$ eV^2 in Fig. 8. The almost horizontal bin $(-0.1 < \cos\theta < 0.0)$ corresponds to a pathlength $L \sim 1000$ km. For $\Delta m^2 \leq 0.01$ eV^2, this is short enough so that the oscillation probability remains small over the relevant region of neutrino energy, $\sim$ 100 GeV (see the "through-going" curve of Fig. 2). For much of the remaining solid angle, however, L $\sim 10^4$ km, and oscillations would occur, given the large mixing angles assumed here. This in turn leads to a relatively uniform suppression of the upward ν_μ flux over most of the angular region, but not for the nearly horizontal directions. Note also that the conclusion one reaches from comparison to the observed angular distribution will depend strongly on the measured fluxes in the two almost horizontal zenith angle bins, which raises questions concerning both statistical and systematic errors. It is therefore not surprising that the χ^2 values obtained for the renormalized angular distributions in Table IV show less sensitivity than those in which the absolute rate information is included.

Stopping Fraction of Upward Muons and Neutrino Oscillations

As noted earlier, the uncertainties in the calculated stopping fraction of upward muons due to uncertainties in the input data are expected to be less than those in the calculations of through-going muons. The former uncertainties are those that affect the energy-dependence of the upward muon spectrum, such as the uncertainty in the slope of the primary energy spectrum and the production of kaons. Table V shows the stopping fraction, defined as stopping/through-going, calculated for the Kamiokande detector.[1] Note that the spread of the calculated values of the stopping fraction in Table V is then about 7%, which is similar in magnitude to our estimation of the overall uncertainty in the input data to the calculations. Accordingly, we take the 7% spread as the measure of uncertainty in the calculated stopping fraction.

In Fig. 9 we show the constraints on neutrino oscillations from stopping muons in a way that is relatively independent of the exact definition of "stopping". For each grid point in the $\Delta m^2 - \sin^2 2\theta$ space we calculate the stopping fraction normalized to the stopping fraction calculated in the absence of oscillations. The figure shows contours of constant values of the ratio stopping fraction $(\Delta m^2, \sin^2 2\theta)$/stopping fraction (no-oscillations). To illustrate the application of Fig. 9 to an experimental result, we find the approximate contour corresponding to that obtained from the measured stopping fraction in IMB [8], 0.16 ± 0.019 relative to the expected fraction, also equal to 0.16. Adding in quadrature a 7% estimated uncertainty in the calculated stopping fraction to the statistical uncertainty in

[1]The analysis of stopping muons for Kamiokande has not yet been completed. For the moment we use a criterion for a stopping muon which corresponds approximately to $1 < E_\mu < 3$ GeV. From Fig. 6, this yields the stopping/through-going ratio as approximately 0.29. The criterion for stopping muons in IMB [8] is that essentially no light be produced in the last five meters of projected track length through the detector. If we estimate the average projected pathlength through the IMB detector as 20 m, stopping muons are those that propagate less than 15 m or have $E_\mu \lesssim 3$ GeV. The minimum muon energy (averaged over IMB 1,2 and 3) is about 1.4 GeV [8]. The ratio stopping/through-going in this energy range from Fig. 6 is 0.19, comparable to the value 0.16 ± 0.019 measured by IMB.

the measurement yields a resultant uncertainty of 18% at 90% c.l. (Note that here the measurement error is larger than the calculational error, unlike the situation in the throughgoing muons.) Thus the 90% c.l. contour corresponds to the curve labelled 0.82 in Fig. 9 a, in satisfactory agreement with curve B, Figure 2 of reference [8]. For completeness, the contours derived from the Bartol flux are shown in Fig. 9b.

The shape of the contours in Fig. 9 can be understood qualitatively from Eq. 2 by comparing the oscillation probability at $E_\nu \sim 10$ GeV, characteristic of stopping muons, with that at $E_\nu \sim 100$ GeV, characteristic of throughgoing muons. For example, if $\Delta m^2 \sim 10^{-3}$ eV^2 (and $L \sim 10^4$ km), the oscillation probability is relatively large for $E_\nu \sim 10$ GeV but negligible for $E_\nu \sim 100$ GeV. This would yield a significant distortion of the upward muon energy spectrum and hence an anomaly in the stopping fraction for the large mixing angles considered here. On the other hand, if $\Delta m^2 \gtrsim 10^{-2}$, then both the high and low energy regions will be affected similarly, and no constraint on Δm^2 will be forthcoming from the stopping fraction. If Δm^2 is too small ($\lesssim 2 \times 10^{-4}$ eV^2), then even the low energy neutrinos will have small neutrino oscillation probability in 10^4 km, and there will again be no constraint.

The relatively small uncertainty in the calculated no-oscillation stopping fraction suggests that the neutrino oscillation information extracted from the stopping fraction data is likely to be definitive in allowing or excluding certain regions in the $\Delta m^2, \sin^2 2\theta$ space. At present, the statistical error in the measured stopping fraction is somewhat larger than the uncertainty in the calculated no-oscillation fraction. Consequently, larger statistical samples, which may be available in the future, will provide significant improvement in the delineation of neutrino oscillations.

Summary

Most previous analyses of upward muons have been based on a relatively early neutrino flux calculation [18], and on a set of structure functions [26] which underestimates more recent neutrino total cross section measurements. Because that combination of neutrino flux and neutrino cross sections from which conclusions relating to neutrino oscillations have previously been extracted [7,8,9] is the lowest of several extant calculations, it appears that the region of the $\Delta m^2, \sin^2 2\theta$ parameter space for ν_μ-disappearance excluded by analyses of upward, through-going muons has been overestimated. Indeed, more recent representations of the neutrino flux and neutrino cross sections lead to oscillation limits from through-going muons that are consistent with the allowed region obtained from the contained event data.

The calculated fraction of muons of lower energy that stop in the detector is subject to smaller uncertainties than the absolute rate of through-going muons. As a consequence, the region in the neutrino oscillation $\Delta m^2 - \sin^2 2\theta$ space delineated by the comparison of the observed stopping fraction with calculation is less ambiguous, and the result is comparable in quality with that obtained from the atmospheric neutrino-induced contained event analysis. Moreover, the present result [8] from the stopping fraction is limited primarily by statistical uncertainty, so there is good prospect for future improvement.

The situation at present with respect to neutrino oscillations in the ν_μ-disappearance and $\nu_\mu \leftrightarrow \nu_\tau$ modes is summarized in Fig. 10. It remains as a challenge to explore further the allowed region suggested by analysis of the contained events [2,6]

We have benefited from comments and criticisms from R. Fletcher, T. Haines, T. Kajita, J. Morfin, J.F. Owens, C. Quigg, J. Stirling, R. Svoboda, W-K. Tung, J. VanderVelde, and D.H. White.

Table I. Muon/Electron event ratios from the KAM [2] and IMB [1] detectors. $R_{data}(\frac{\mu}{e})$ and $R_{MC}(\frac{\mu}{e})$ are the measured and Monte Carlo calculated ratios of muons to electron in the momentum intervals indicated in the last column. $R_{MC}^{data}(\frac{\mu}{e})$ is the ratio of the entries in rows 1 and 2.

Ratio	KAM 4.9 kton-yr	IMB 7.7 kton-yr	Conditions
$R_{data}(\frac{\mu}{e})$	0.72 ± 0.09	0.56 ± 0.05	$100 < p_e < 1200$ MeV/c $300 < p_\mu < 1200$ MeV/c
$R_{MC}(\frac{\mu}{e})$	1.11	1.04	as in $R_{data}(\frac{\mu}{e})$
$R_{MC}^{data}(\frac{\mu}{e})$	$0.65 \pm 0.08 \pm 0.06$	$0.54 \pm 0.05 \pm 0.12$	$100 < p_e < 1200$ MeV/c $300 < p_\mu < 1200$ MeV/c

Table II. The calculated ratio $R_\nu \equiv \phi(\nu_e + \bar{\nu}_e)/\phi(\nu_\mu + \bar{\nu}_\mu)$ obtained from the neutrino flux calculations in the cited references for the interval $0.1 \lesssim E_\nu \lesssim 1.5$ GeV. There is a small energy dependence of R_ν above the energy interval specified.

Reference	Method	Interaction model	R_ν
G. Barr, Gaisser & Stanev [11]	M.C.	Parametrized data	0.48
Lee & Koh [12]	M.C.	"	0.48
Honda, Kasahara *et al.* [13]	M.C.	NUCRIN + LUND	0.46
Kawasaki & Mizuta[14]	analytic	Analytic parametrization	0.49

Table III. Throughgoing muon fluxes at Kamiokande for four different neutrino fluxes and two sets of structure functions: (a) Owens[27] and (b) EHLQ2[26]. The muon fluxes (column 2 and 3) are given in units of $cm^{-2}sr^{-1}s^{-1} \times 10^{13}$. The asterisks are explained in the text.

Reference	*Muon Flux*		*R(meas/calc)*	
	(a)	(b)	(a)	(b)
Bartol[21]	2.36	2.11	0.86	0.97
Butkevich[20]	2.43	2.16	0.84	0.94
Mitsui[19]	2.30	2.05[*]	0.89	1.00
Volkova[18]	2.18	1.95[*]	0.94	1.05

Table IV. χ^2 values for fits of the calculated distributions of Fig. 8a (column 3) and Fig. 8b (column 4) to the Kamiokande data. The columns under (shape only) are the χ^2 values after renormalizing each curve in Figs. 8a and 8b to the same total signal as the data.

		χ^2			
$\sin^2 2\theta$	$\Delta m^2(eV^2$	(a)	(b)	(a)	(b)
				(Shape only)	
0.5	0.01	10.3	14.6	10.3	9.5
0.8	0.0046	10.0	19.1	9.9	11.6
0.5	0.10	10.9	19.5	9.2	7.8
0.0	0.0	18.2	8.7	9.5	8.7

Table V. Calculated stopping fractions (stopping/through-going) from the neutrino flux calculations and structure functions (a) [27] and (b) [26].

	stop/through	
Reference	(a)	(b)
Bartol[21]	0.28	0.28
Butkevich[20]	0.30	0.30
Mitsui[19]	0.30	0.30
Volkova[18]	0.30	0.30

References

[1] R. Becker-Szendy et al. (IMB Collaboration), Phys. Rev. D46, 3720 (1992). See also D. Casper *et al.* Phys. Rev. Letters 66 (1991) 2561.

[2] K.S. Hirata *et al.* (Kam-II Collaboration), Physics Letters B 280 (1992) 146.

[3] K.S. Hirata *et al.* Physics Letters B 205 (1988) 416.

[4] Ch. Berger *et al.* Physics Letters B 245 (1990) 305 and 227 (1989) 489.

[5] M. Aglietta *et al.* Europhysics Letters 8 (1989) 611.

[6] E.W. Beier *et al.* Physics Letters B 283 (1992) 446.

[7] M.M. Boliev *et al.* (Baksan Collaboration) in Proc. 3rd Int. Workshop on Neutrino Telescopes (ed. Milla Baldo-Ceolin) (1991), 235.

[8] R. Becker-Szendy *et al.* (IMB Collaboration) Phys. Rev. Letters 69 (1992) 1010.

[9] M. Mori *et al.* (Kamiokande Collaboration) Physics Letters B270 (1991) 89. See also M. Mori, to be published in Proc. High Energy Neutrino Astrophysics Workshop (Univ. of Hawaii, March 1992, ed. V.J. Stenger, J.G. Learned, S. Pakvasa & X. Tata, World Scientific, Singapore).

[10] Y. Oyama *et al.* (Kamiokande Collaboration) Phys. Rev. D39 (1989) 1481. See also [24].

[11] G. Barr, T.K. Gaisser & Todor Stanev, Phys. Rev. D39 (1989) 3532.

[12] H. Lee & Y.S. Koh, Nuovo Cimento B 105 (1990) 883.

[13] M. Honda, K. Kasahara, K. Hidaka & S. Midorikawa, Physics Letters B 248 (1990) 193.

[14] M. Kawasaki & S. Mizuta, Phys. Rev. D43 (1991) 2900.

[15] E.V. Bugaev & V.A. Naumov, Physics Letters B 232 (1989) 391.

[16] L.V. Volkova in *Cosmic Gamma Rays, Neutrinos and Related Astrophysics* (ed. M.M. Shapiro & J.P. Wefel) NATO ASI vol. 270, p. 139 (1989).

[17] T.K. Gaisser in Proc. Conf. on Long Baseline Neutrino Oscillations (Fermilab, Nov. 17-21, 1991) (ed. M. Goodman) p. 111.

[18] L.V. Volkova, Yad. Fiz. 31 (1980) 784 (Sov. J. Nucl. Phys. 31 (1980) 1510).

[19] K. Mitsui, Y. Minorikawa & H. Komori, Nuovo Cimento 9C (1986) 995.

[20] A.V. Butkevich, L.G. Dedenko & I.M. Zheleznykh, Yad. Fiz. 50 (1989) 142 (Sov. J. Nucl. Phys. 50 (1989) 90).

[21] V. Agrawal, T.K. Gaisser, Paolo Lipari & T. Stanev, in preparation. Note that the best estimate of the flux shown here is somewhat lower ($\sim$ 6%) than the flux shown in a draft version of this paper. That flux was an estimate of the highest neutrino flux consistent with the measurements of muon fluxes.

[22] O.C. Allkofer & P.K.F. Grieder, *Cosmic Rays on Earth* (Number 25-1 of Physik Daten, Fachinformationszentrum, Karlsruhe, 1984).

[23] Paolo Lipari & Todor Stanev, Phys. Rev. D44 (1991) 3543.

[24] Y.Oyama, Univ. of Tokyo Thesis (ICR-Report-193-89-10) (1989).

[25] W. Lohmann, R. Kopp & R. Voss, CERN Yellow Report No. EP/85-03.

[26] E. Eichten, I. Hinchcliffe, K. Lane & C. Quigg, Revs. Mod. Phys. 56 (1984) 579 (Erratum 58 (1986) 1065).

[27] J.F. Owens, Physics Letters B 266 (1991) 126.

[28] J. Morfin & W. Tung, Z. Phys. C 52 (1991) 13.

[29] J. Kwiecinski, A.D. Martin, W.J. Stirling & R.G. Roberts, Phys. Rev. D42 (1990), 3645.

[30] Phys. Rev. D45 III.82 (1992).

[31] R. Field & R.P. Feynman, Phys. Rev. D15 (1977) 2590.

[32] R. Becker-Szendy *et al.*, Singapore High Energy Physics Conference, p.662, (1990).

Figure Captions

Fig. 1. Neutrino oscillation ($\Delta m^2, \sin^2 2\theta$) plot for the ν_μ-disappearance mode showing the region (cross hatched) allowed by the atmospheric neutrino contained event data of reference [2] delimited by accelerator experiments [CDHS Collaboration, F. Dydak *et al.*, Phys. Lett. B134, 281 (1984).], [CHARM Collaboration, F. Bergsma *et al.*, Phys. Lett. B142, 103 (1984)] and the Fréjus underground detector [4].

Fig. 2. Approximate energies of atmospheric neutrinos giving rise to the contained events, and the upward stopping and through-going muons in an underground detector.

Fig. 3. (a). Calculated neutrino flux, $\phi(\nu_\mu + \bar{\nu}_\mu)$, as a function of E_ν from reference [21]. (b) Ratios of calculated fluxes $\Phi(\nu_\mu + \bar{\nu}_\mu)$ from references [18,19,20] relative to the flux from reference [21].

Fig. 4. Zenith angle distributions of the upward through-going muons. The histograms are calculated for the Kamiokande detector from the four calculated neutrino fluxes in Fig. 3 and the Owens [27] structure functions. The points are the Kamiokande data [9].

Fig. 5. Plot comparing the calculated neutrino and antineutrino total cross sections as functions of E_ν obtained from the indicated nucleon structure functions with the world data [30].

Fig. 6. Calculated through-going fluxes as a function of effective muon threshold energy obtained from the neutrino fluxes in Fig. 3 and the Owens structure functions [27].

Fig. 7. $\Delta m^2, \sin^2 2\theta$ space showing the cross-hatched region allowed by the contained event data from Fig. 2. The excluded regions to the right of the contours marked IMB [8] and KAM [9] are reproduced from their analyses of upward through-going muons based on the Volkova neutrino flux [18] and the EHLQ 2 [26] structure functions. The

calculated contour for the Kamioka data with Bartol neutrino flux and Owens structure functions is marked KBO. See the text for discussion of the KAM [9] contour in relation to the contour marked KVE calculated by us for the Kamioka data with the Volkova flux and EHLQ2 structure functions.

Fig. 8. Calculated zenith angle distributions of upward through-going muons with neutrino oscillations included, corresponding to three parameter pairs $(\Delta m^2, \sin^2 2\theta)$ allowed by the contained event result in Fig. 2. The points are the Kamiokande data. (a) The histograms are based on the Bartol neutrino flux and Owens structure functions. (b) The histograms are based on the Volkova neutrino flux and the EHLQ2 structure functions.

Fig. 9. Plot of calculated Δm^2 *vs* $\sin^2 2\theta$ contours obtained for various assumed values of the fraction of upward stopping muons (stops/through-going), normalized to the calculated fraction in the absence of oscillations. The regions in Δm^2 and $\sin^2 2\theta$ enclosed by the contours are excluded.

Fig. 10. The present situation with respect to neutrino oscillations in the ν_μ-disappearance and $\nu_\mu \leftrightarrow \nu_\tau$ modes. [$(\nu_\mu \rightarrow \nu_\tau)$, N. Ushida *et al*, (FNAL Collaboration), Phys. Rev. Lett. 57, 2897 (1986).]

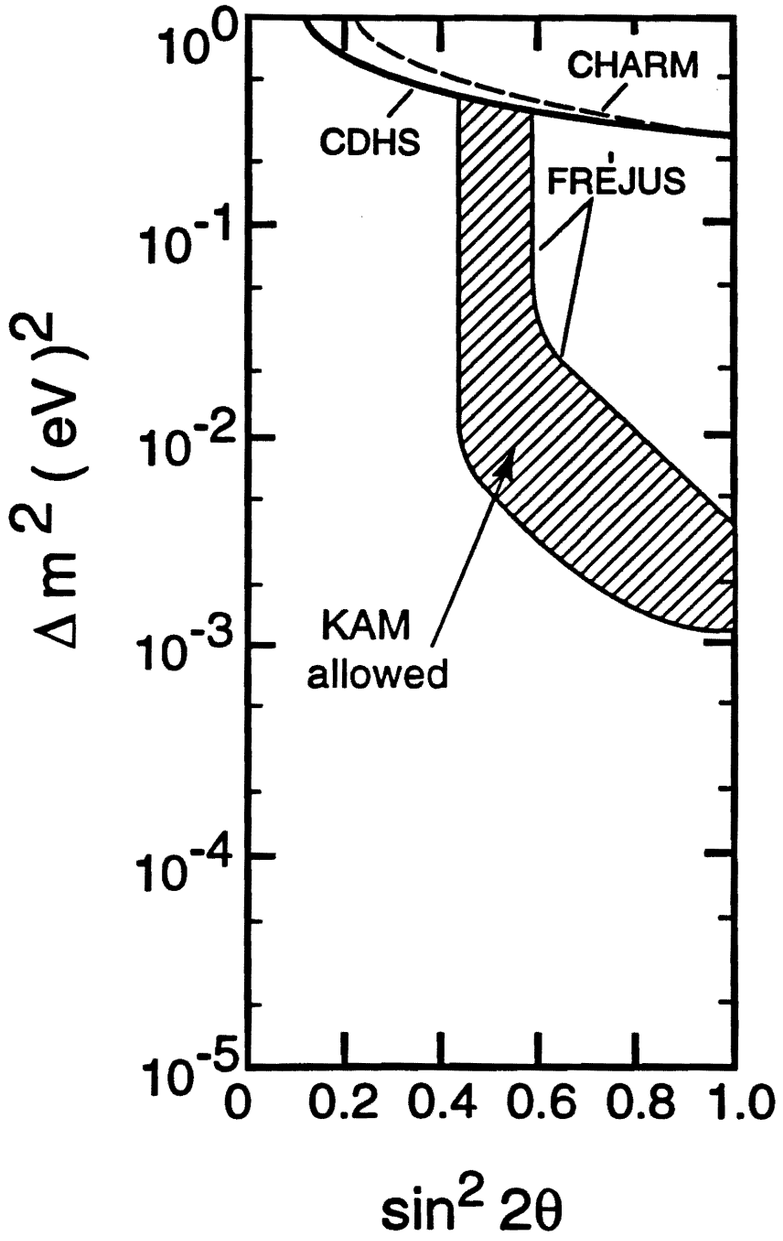

Fig.1

92-0021b

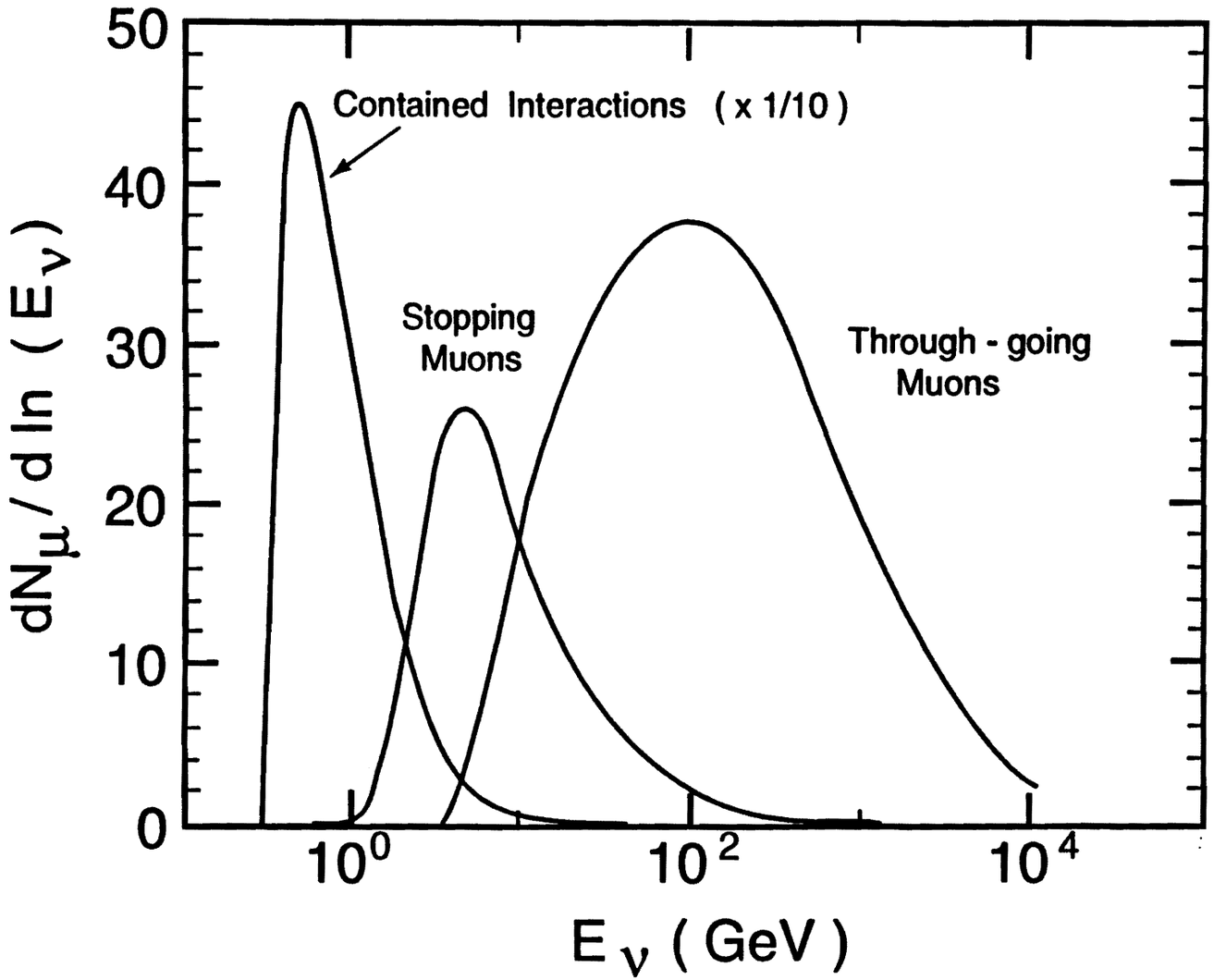

Fig.2

93-0022p

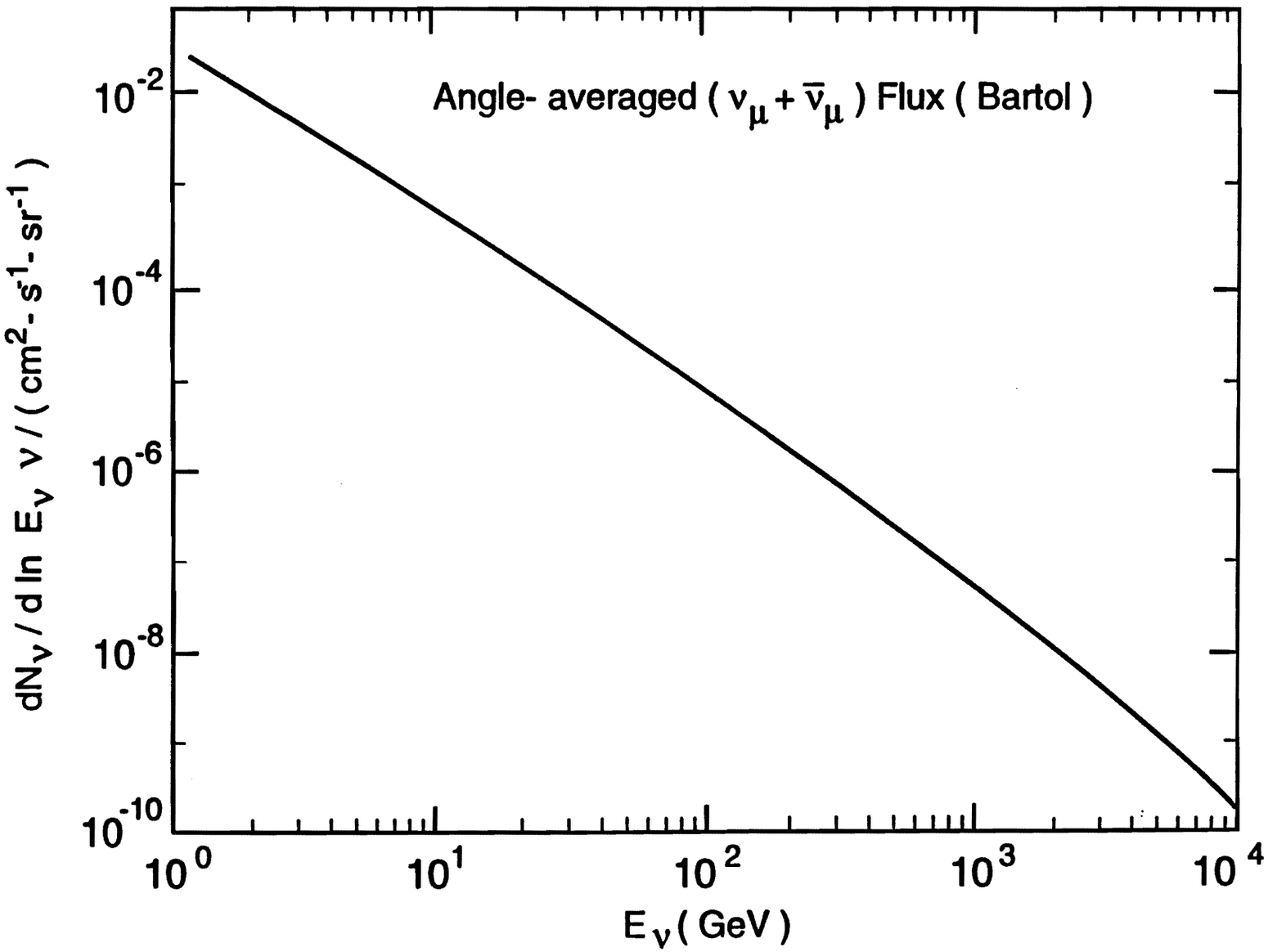

93-0022m

Fig.3a

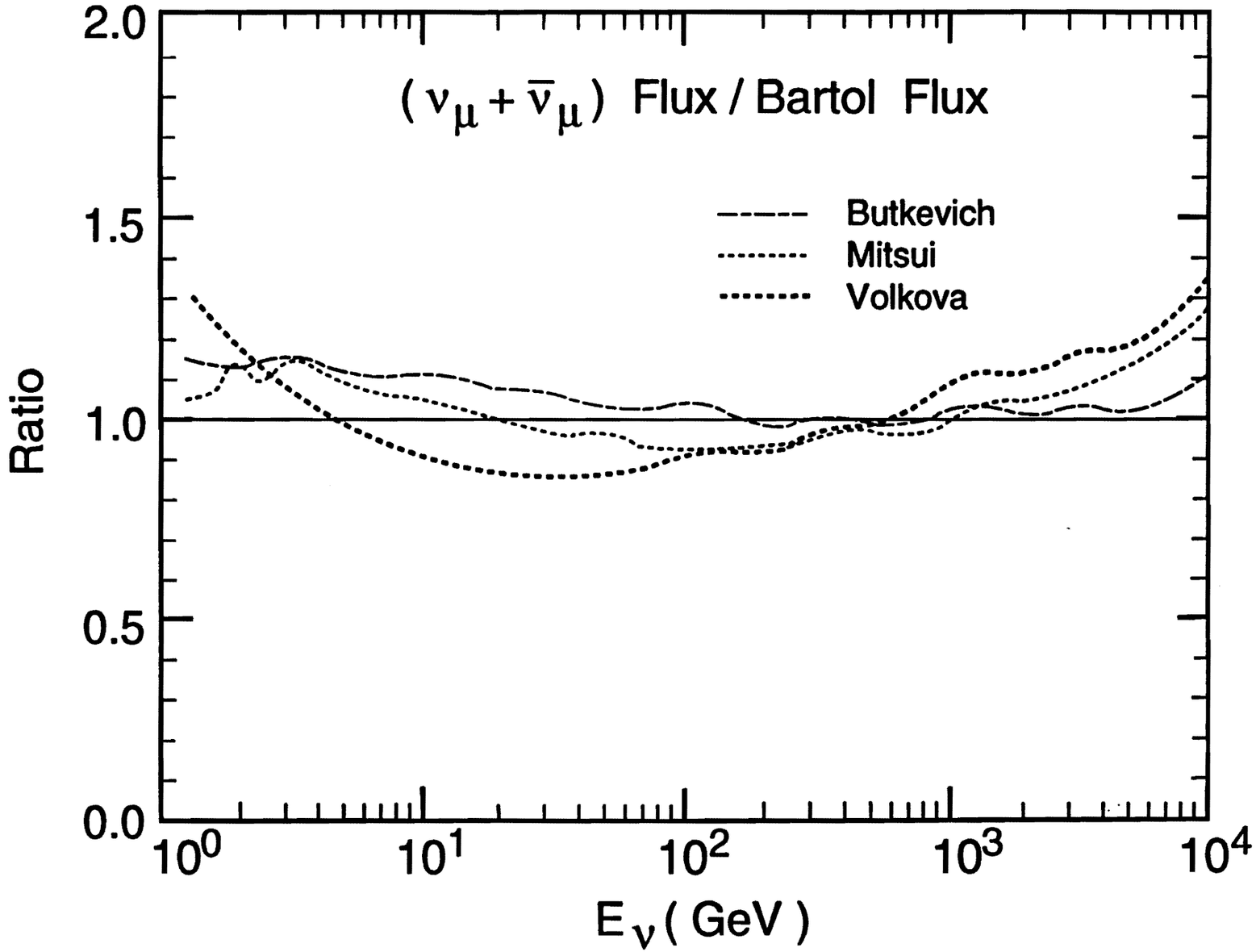

Fig.3b

93-0022L 2

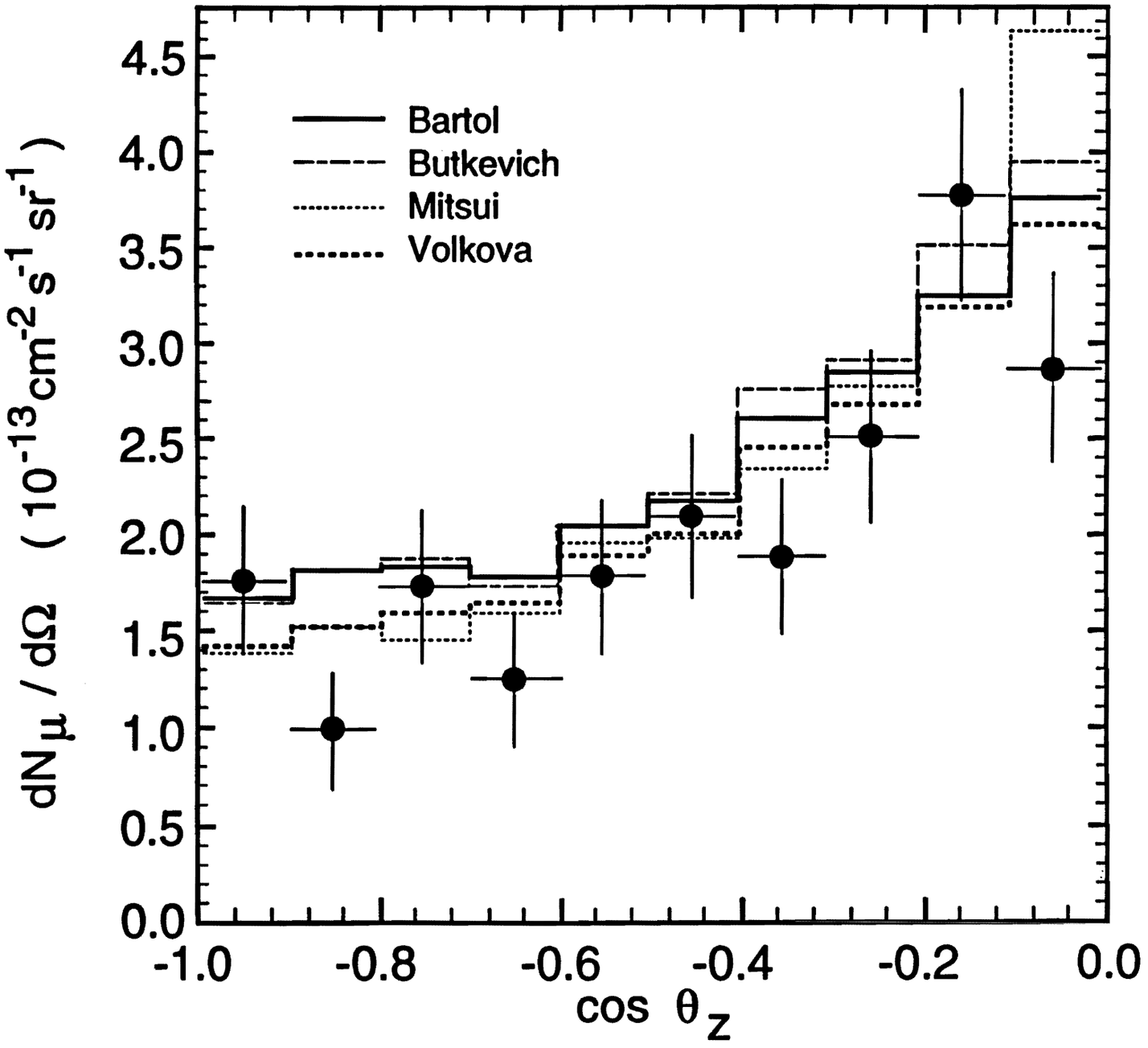

93-0022a 2

Fig.4

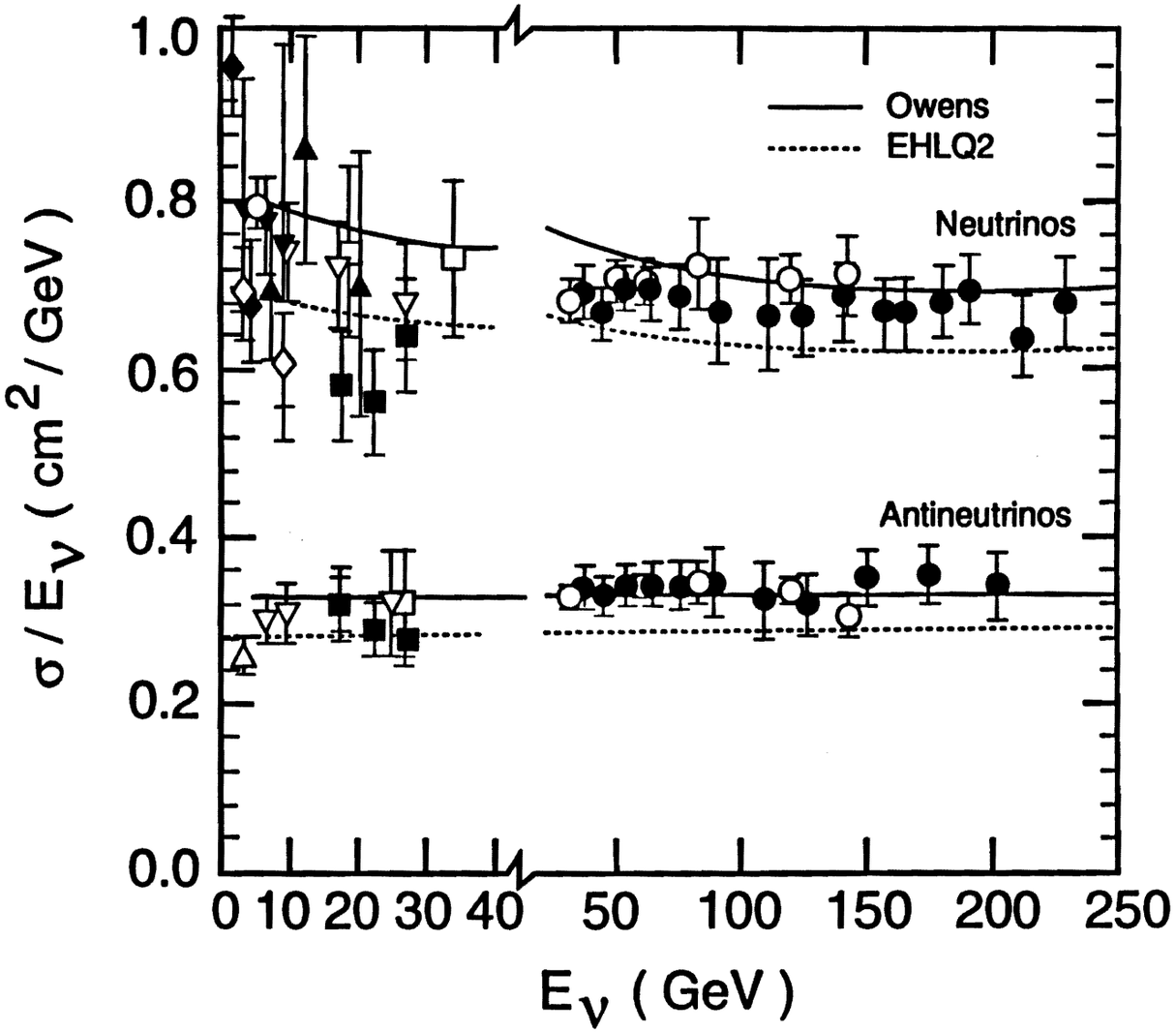

Fig. 5

93-0055g 3

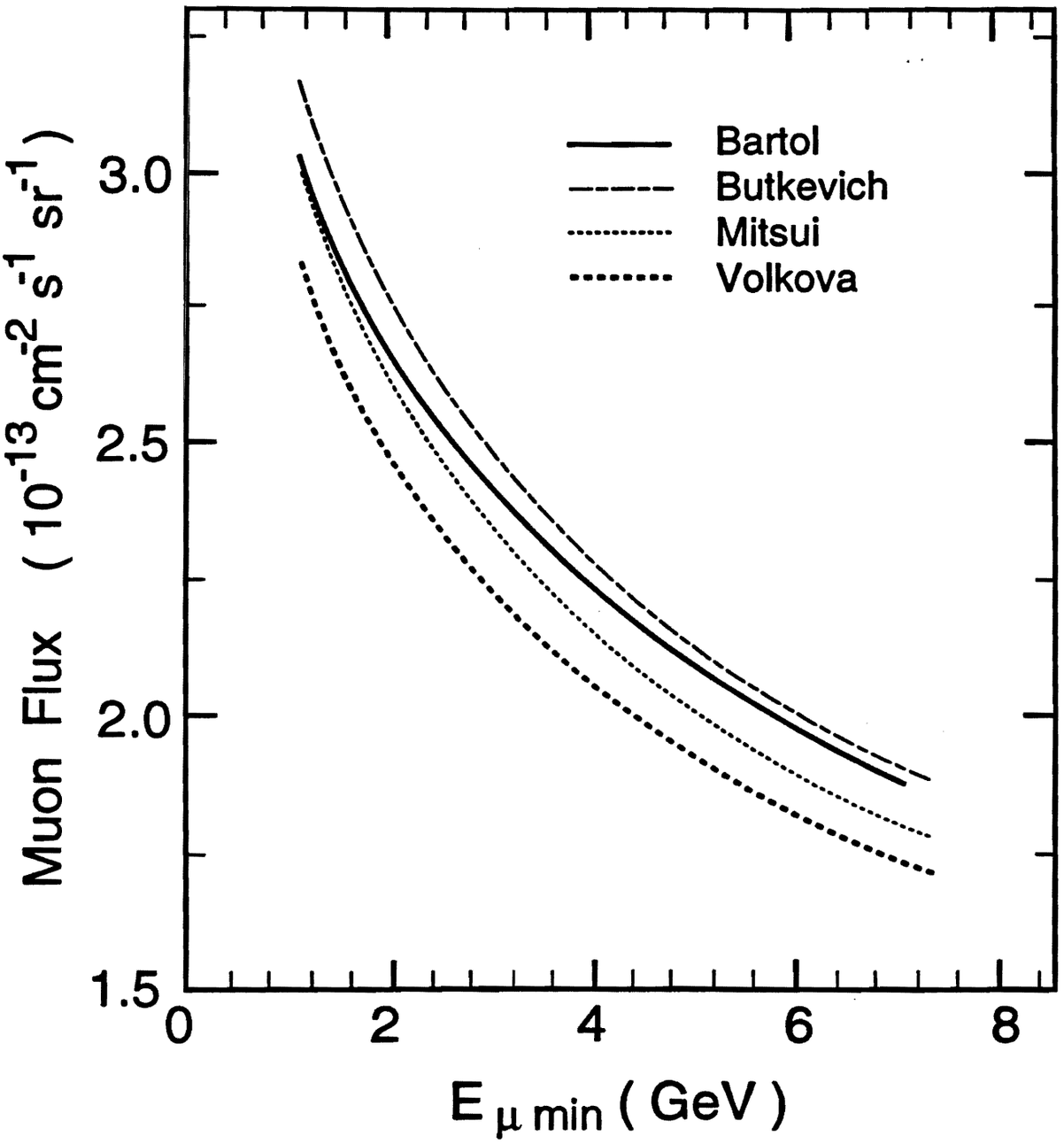
Bartol
Butkevich
Mitsui
Volkova
Muon Flux (10^{-13} cm^{-2} s^{-1} sr^{-1})
3.0
2.5
2.0
1.5
0
2
4
6
8
$E_{\mu\,min}$ (GeV)

Fig. 6

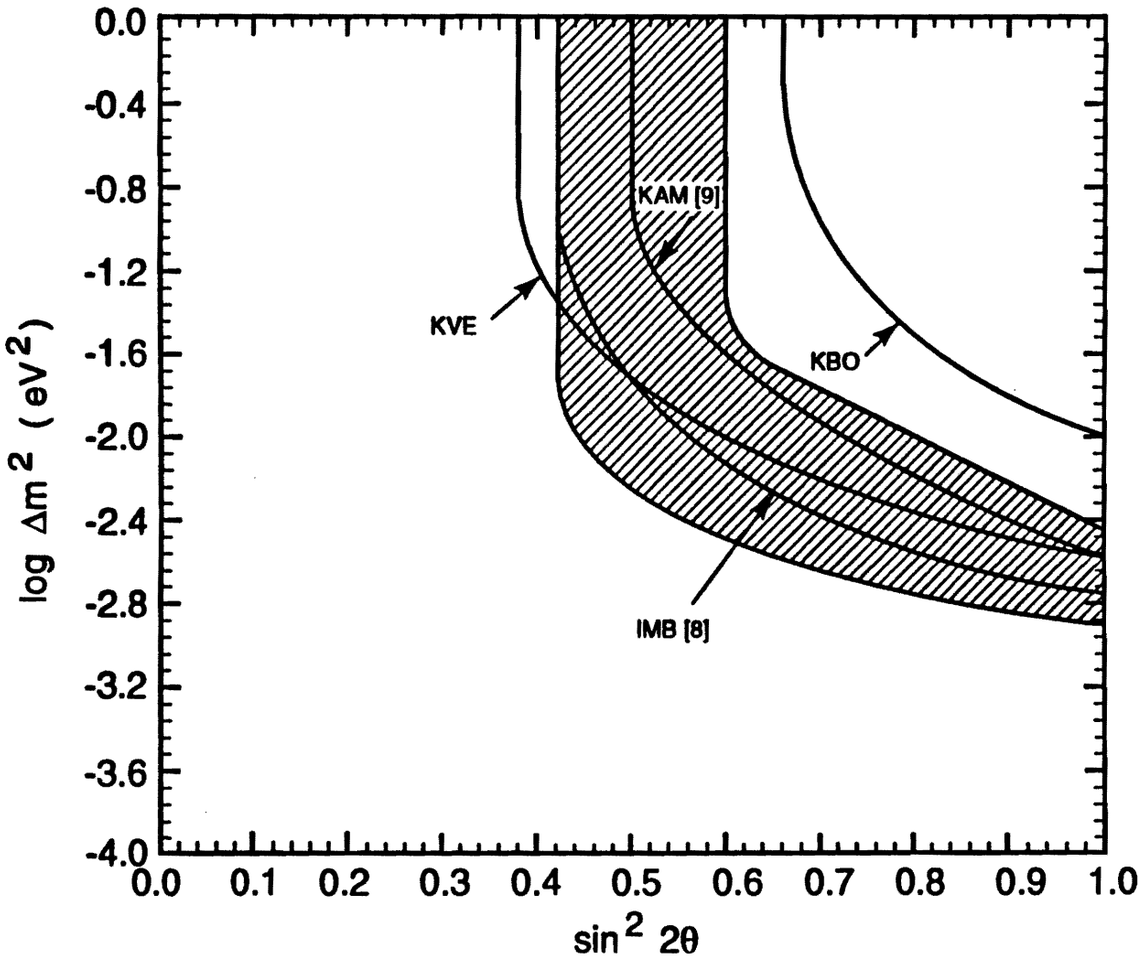
0.0
-0.4
-0.8
-1.2
-1.6
-2.0
-2.4
-2.8
-3.2
-3.6
-4.0
log Δm² (eV²)
0.0
0.1
0.2
0.3
0.4
0.5
0.6
0.7
0.8
0.9
1.0
sin² 2θ
KAM [9]
KVE
KBO
IMB [8]

Fig. 7

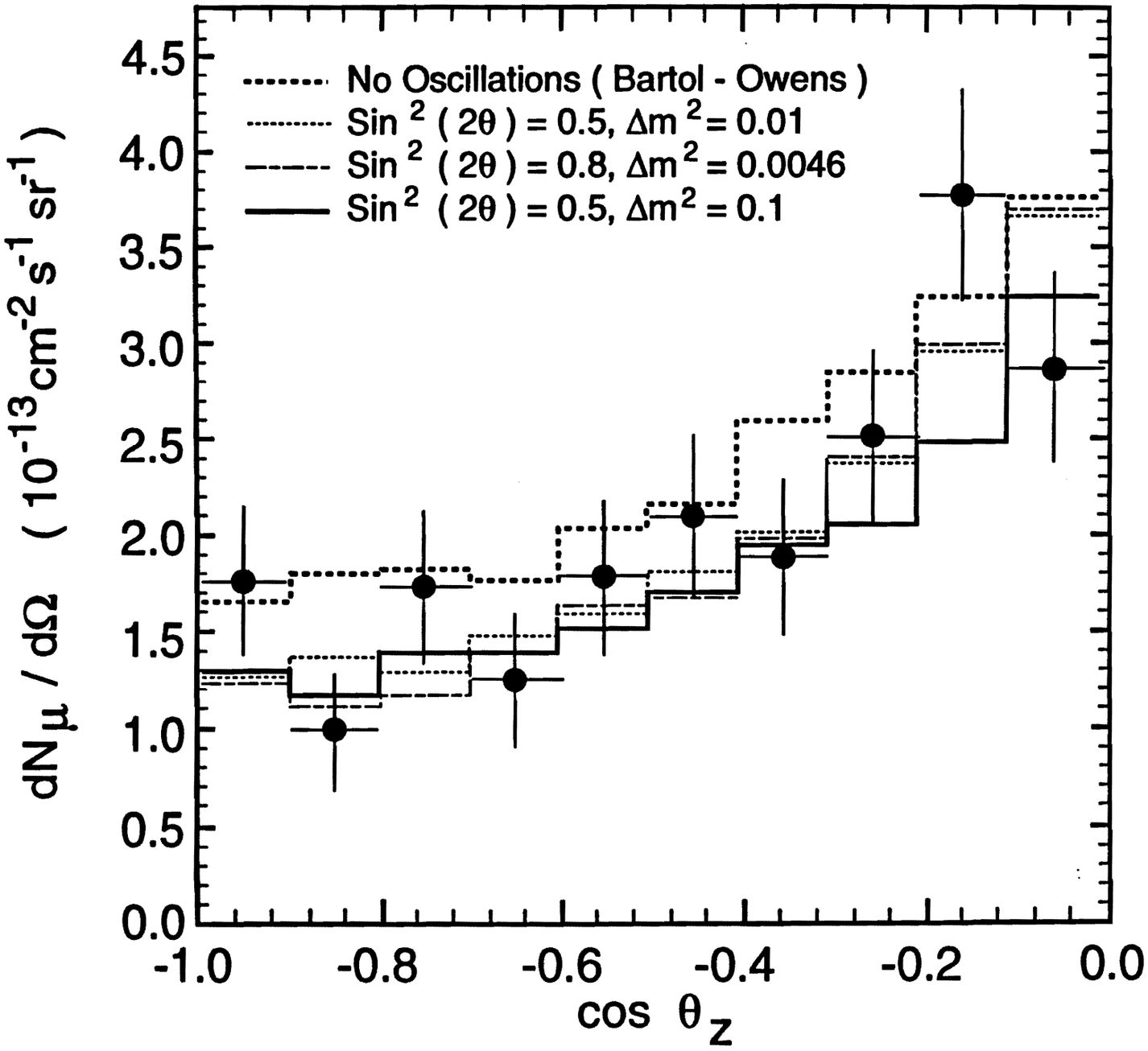

93-0022d 2

Fig.8a

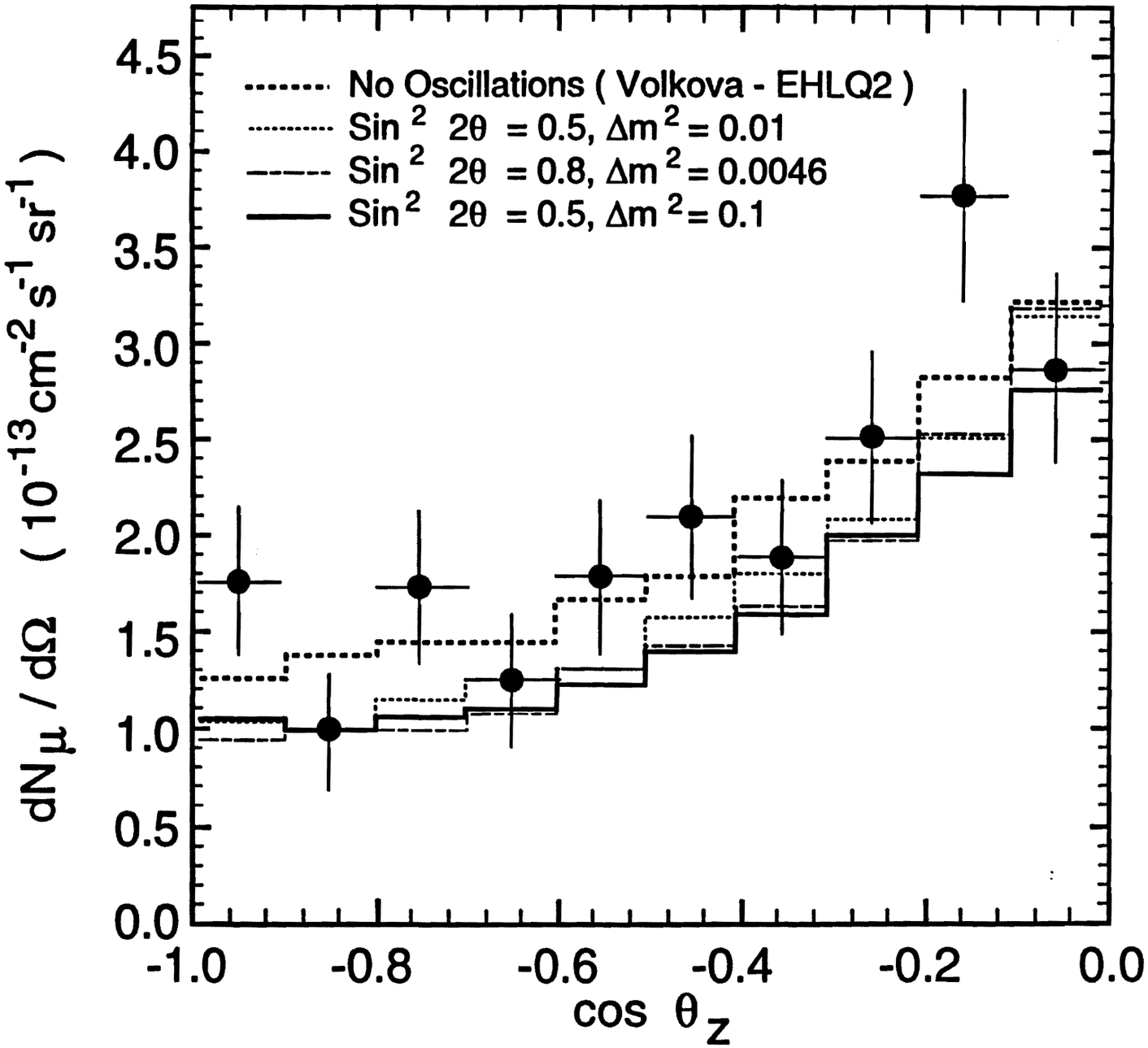

93-0022c (Rev) 2

Fig.8b

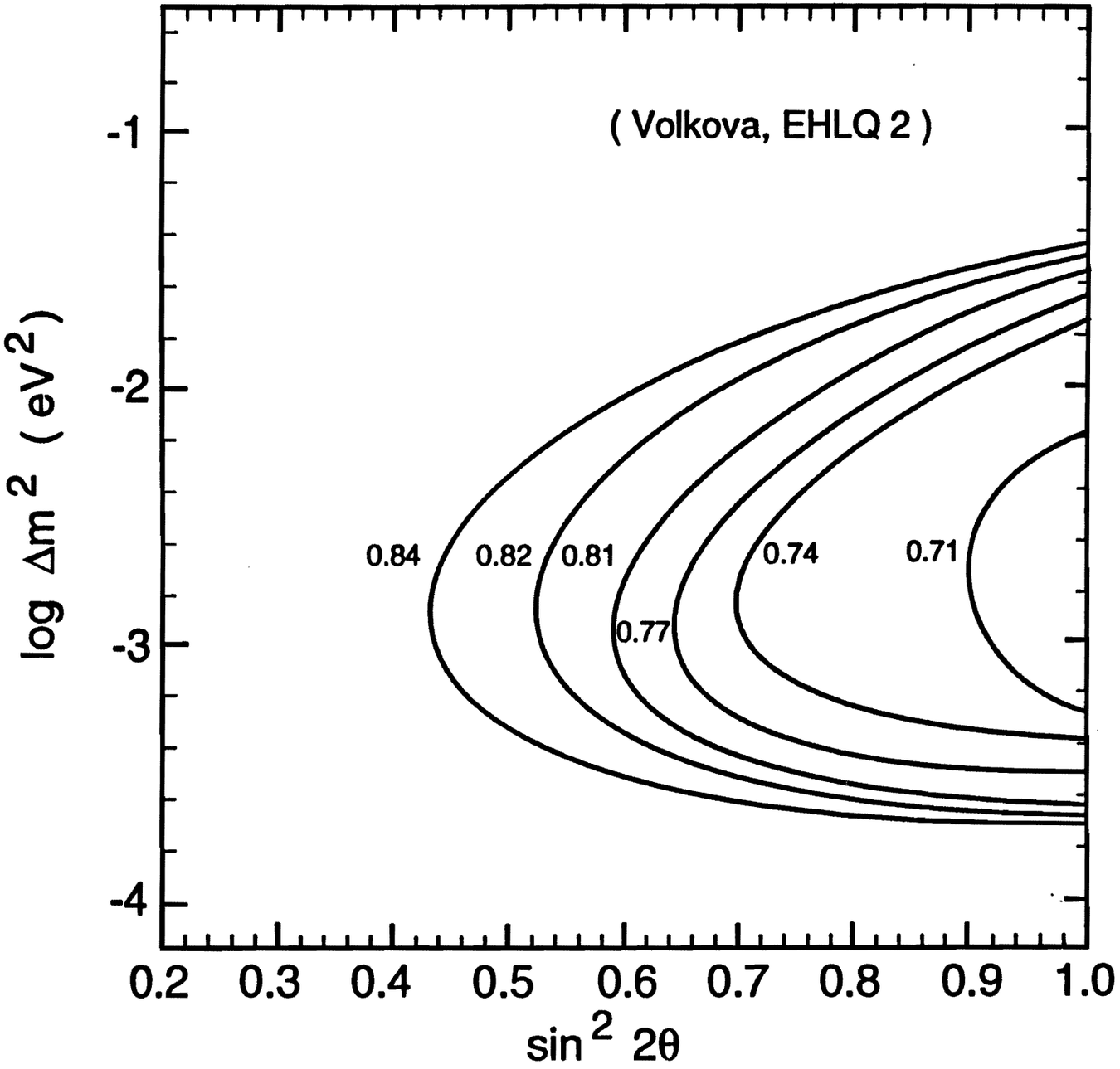

93-0022r 2

Fig. 9a

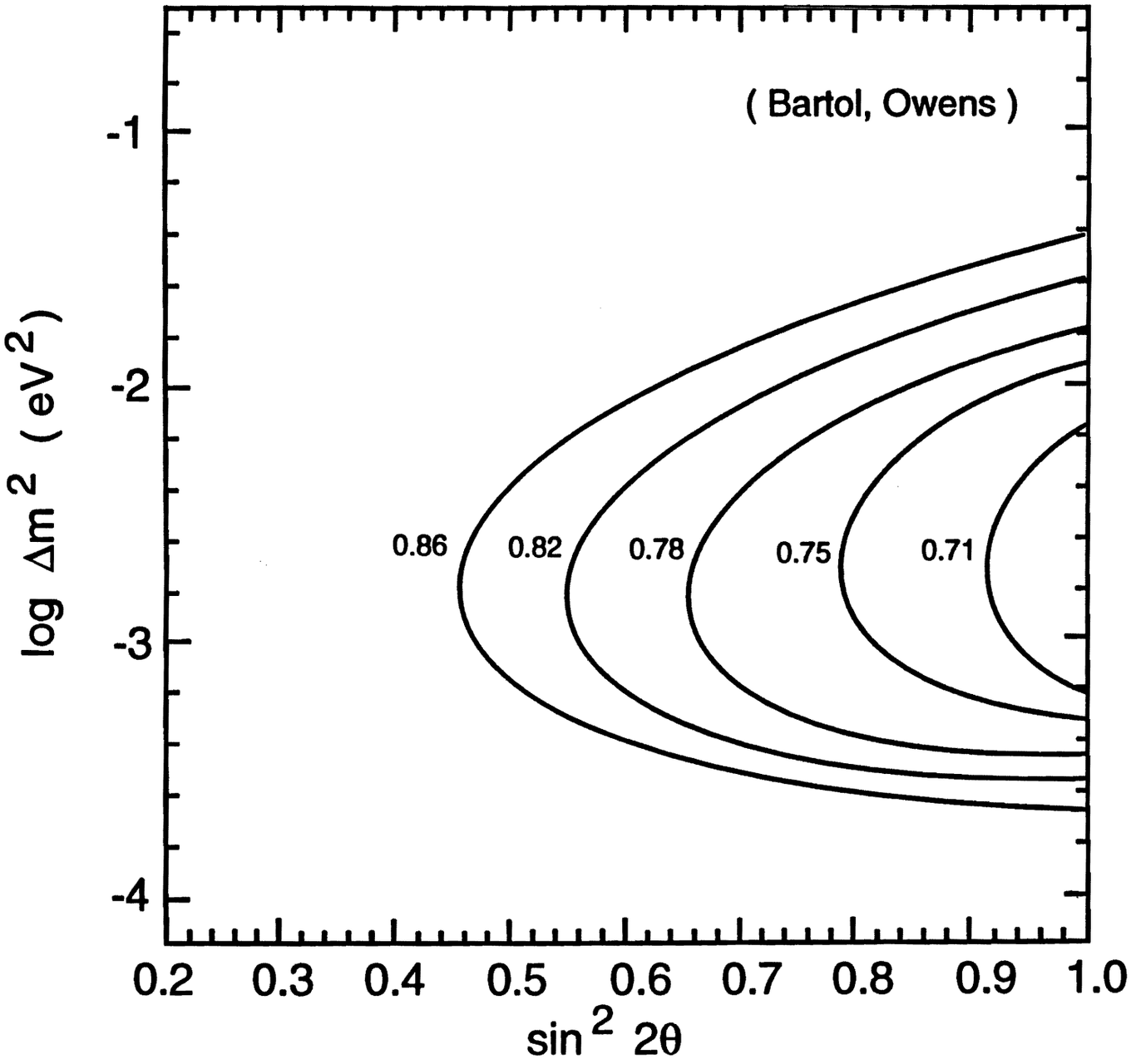

93-0022q 2

Fig. 9b

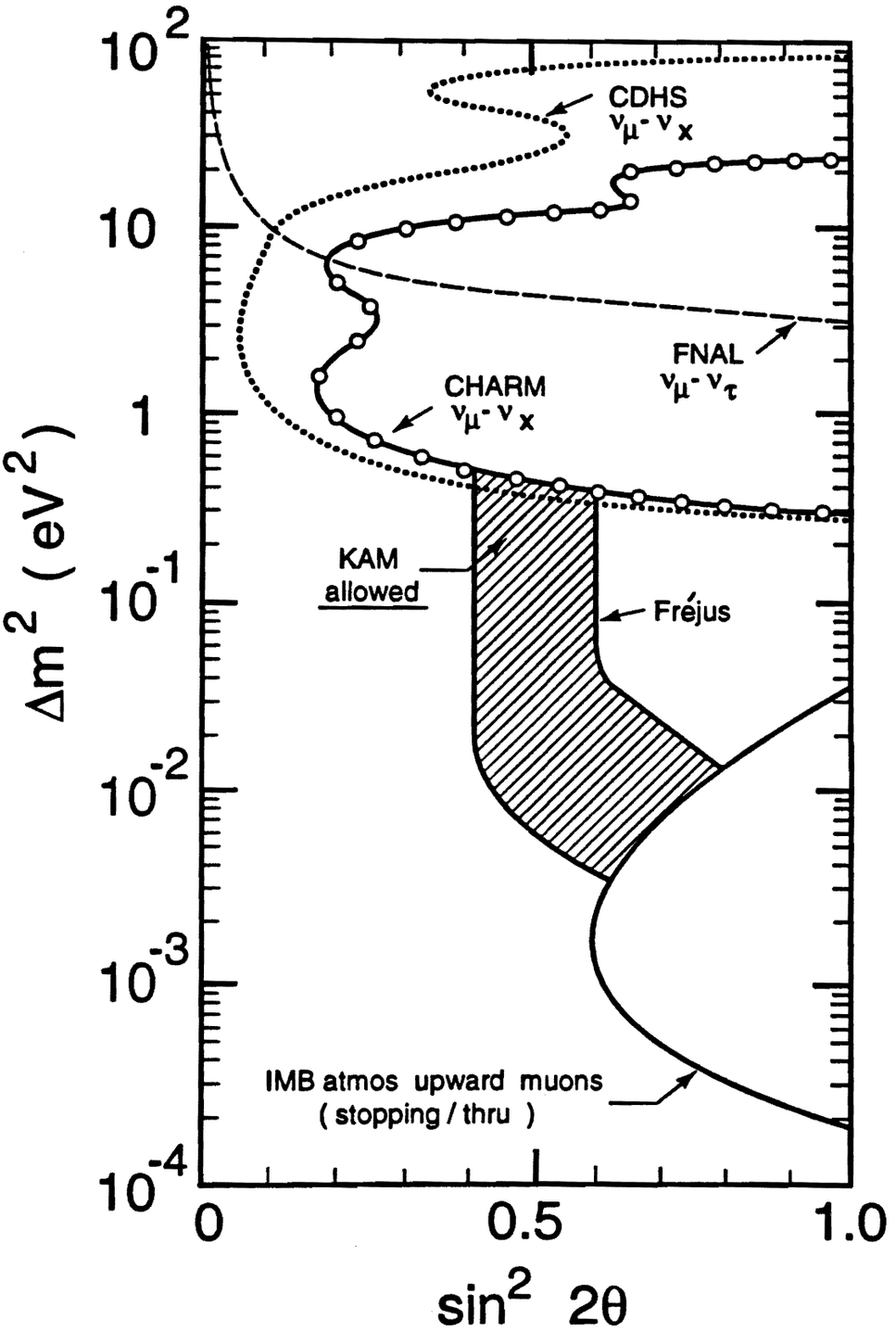
10^2
10
1
10^{-1}
10^{-2}
10^{-3}
10^{-4}
Δm^2 (eV^2)
CDHS
ν_μ - ν_x
FNAL
ν_μ - ν_τ
CHARM
ν_μ - ν_x
KAM
allowed
Fréjus
IMB atmos upward muons
(stopping / thru)
0
0.5
1.0
$\sin^2 2\theta$

Fig. 10